AUTHOR QUERY FORM

ELSEVIER	**Journal:** ELSPEC **Article Number:** 45877	**Please e-mail or fax your responses and any corrections to:** **E-mail:** corrections.esil@elsevier.thomsondigital.com **Fax:** +353 6170 9272

Dear Author,

Please check your proof carefully and mark all corrections at the appropriate place in the proof (e.g., by using on-screen annotation in the PDF file) or compile them in a separate list.

For correction or revision of any artwork, please consult http://www.elsevier.com/artworkinstructions.

Any queries or remarks that have arisen during the processing of your manuscript are listed below and highlighted by flags in the proof. Click on the 'Q' link to go to the location in the proof.

Location in article	Query / Remark: click on the Q link to go Please insert your reply or correction at the corresponding line in the proof
Q1	Please provide 3–5 Research Highlights. For more information, see www.elsevier.com/researchhighlights.

Thank you for your assistance.

Journal of Electron Spectroscopy and Related Phenomena xxx (2010) xxx–xxx

Contents lists available at ScienceDirect

Journal of Electron Spectroscopy and Related Phenomena

journal homepage: www.elsevier.com/locate/elspec

Comparison of the electronic structure of $LnBaCo_2O_{5+\delta}$ (Ln = Gd; Dy; Ln-112) and $LnBaCo_4O_7$ (Ln = Yb; Ln-114) single-crystal surfaces using resonant photoemission

H.M. Rafique[a], W.R. Flavell[a,*], A.G. Thomas[a], K.L. Syres[a], S.N. Barilo[b], S.V. Shiryaev[b], G.L. Bychkov[b], D.M.P. Holland[c], A.E.R. Malins[c], G. Miller[c], V.R. Dhanak[c]

[a] School of Physics & Astronomy and The Photon Science Institute, The University of Manchester, Oxford Road, Manchester, M13 9PL, UK
[b] The Institute of Solid State and Semiconductor Physics, Belarussian Academy of Science, 17 P. Brovka St., Minsk 220072, Belarus
[c] STFC Daresbury Laboratory, Daresbury, Warrington, Cheshire, WA4 4AD, UK

ARTICLE INFO

Q1 *Article history:*
Available online xxx

Keywords:
Resonant photoemission
Cobalt oxide
$LnBaCo_2O_{5+\delta}$ (Ln = Gd
Dy
Ln-112)
$LnBaCo_4O_7$ (Ln = Yb
Ln-114)
Metal–insulator transition

ABSTRACT

A comparison of the electronic structure of $LnBaCo_2O_{5+\delta}$ (Ln = Gd, Dy; Ln-112) and $LnBaCo_4O_{7+\delta}$ (Ln = Yb; Ln-114) single-crystal surfaces has been made using synchrotron photoemission spectroscopy. Resonant photoemission is used to identify the atomic parentage of the valence band states of Ln-114. The states close to the Fermi energy are found to be of mixed Co 3d/O 2p character. Comparison of the photoemission results for the two systems allows unambiguous identification of the spectral signal due to low spin octahedral Co^{3+} in Ln-112. High resolution valence band spectra taken as a function of temperature reveal the presence of the metal–insulator (MI) transition in Ln-112 in the 300–400 K temperature range. The gradual changes in the spectral profile of the low energy states with temperature rule out a sudden 'high spin–low spin' switch as the mechanism of the MI transition. They are instead consistent with a gradually shifting equilibrium between three states—low spin, intermediate spin and high spin.

1. Introduction

$LnBaCo_2O_{5+\delta}$ (Ln = lanthanide element, Ln-112) and $LnBaCo_4O_{7+\delta}$ (Ln-114) are highly correlated Co oxides that show potentially useful magnetic and electronic properties. The 'double perovskites' of general formula $LnBaCo_2O_{5+\delta}$ ($0 \leq \delta \leq 1$) show giant magnetoresistive behaviour in narrow composition ranges around $\delta = 0.5$ corresponding to Co^{3+}), a range of poorly-understood spin state transitions, and a temperature-dependent metal–insulator (MI) transition [1–7]. Co^{3+} is present in two environments, octahedral and pyramidal (with CoO_5 coordination) [2]. The temperature-dependent metal–insulator transition is thought to be associated with changes in the spin state of Co^{3+} in the octahedral sites, analogous to the simple perovskite $LaCoO_3$ [8–10]. The latter undergoes Co spin state transitions from low spin (LS, $t_{2g}^6e_g^0$) to high spin (HS, $t_{2g}^4e_g^2$) in the temperature range 90–500 K [10,11], which are thought to proceed via an intermediate spin (IS, $t_{2g}^5e_g^1$) state. In the case of $LnBaCo_2O_{5+\delta}$, however, the mechanism of the transition is a subject of debate, with several different mechanisms, including a sudden LS–HS spin flip, having been proposed [6].

The mixed-valence Kagomé antiferromagnet $LnBaCo_4O_{7+\delta}$, unusually for a cobalt oxide, contains no Co in octahedral environments for low values of δ—instead sheets of CoO_4 tetrahedra, linked in the third dimension by triangular sheets of CoO_4 are present [12–16]. In principle the oxygen content may vary in the range $-0.5 \leq \delta \leq 1.58$ [13], and only when the stoichiometry is forced to $\delta \geq 1$ by oxygen annealing, do Co ions begin to occupy edge-sharing octahedral sites [17]. The transition metal ions in a Kagomé geometry present one of the most highly frustrated two-dimensional quantum spin systems with only nearest-neighbour antiferromagnetic Heisenberg interactions. The system is therefore of fundamental interest, as it presents a good candidate for a chiral-glass-like state with ordered local chirality. It has so far not been studied by photoemission.

Here, we compare the valence band electronic structure of Ln-112 and Ln-114 phases. The absence of octahedral Co^{3+} sites in the latter means that no Co^{3+} LS sites are present. A comparison of the electronic structure of the two phases thus allows us to confirm the assignment of a valence band feature of Ln-112 that has previously been tentatively associated with LS Co^{3+} [1]. We probe the atomic character of the valence band states of Ln-114 using

* Corresponding author. Tel.: +44 161 306 4466; fax: +44 161 275 1001.
E-mail address: wendy.flavell@manchester.ac.uk (W.R. Flavell).

0368-2048/$ – see front matter © 2010 Published by Elsevier B.V.
doi:10.1016/j.elspec.2010.12.012

resonant photoemission, and the metal–insulator transition in Ln-112.

2. Experimental

Single crystals of $LnBaCo_2O_{5+\delta}$ (Ln = Gd, Dy; Ln-112, $\delta \approx 0.5$) and $LnBaCo_4O_{7+\delta}$ (Ln = Yb; Ln-114, $\delta \approx 0.2$) of typical dimension 2 mm × 3 mm × 2 mm were grown from an overstoichiometric melt [7,18,19]. Oxygen content was controlled by post-growth annealing in O_2 or N_2 and measured in typical cases using iodometric titration. The samples were characterised by X-ray and neutron diffraction, and magnetisation measurements [7,19,20].

Resonant photoemission measurements were carried out at the Synchrotron Radiation Source (SRS), STFC Daresbury Laboratory. The beamlines used were the multipole wiggler beamline MPW6.1 (PHOENIX, photon energy range 40 eV ≤ $h\nu$ ≤ 350 eV [21]), with a VG CLAM4 electron energy analyser, and the McPherson 5 m normal incidence high resolution monochromator (5 eV ≤ $h\nu$ ≤ 35 eV) on station 3.2, with a VSW HA100 electron energy analyser. Station 3.2 was used in high resolution mode to detect the small changes occurring near the Fermi energy as a function of temperature. The combined instrumental (monochromator + analyser) resolution in these experiments was 115 meV. Stations 6.1 and 3.2 were also used for valence band photoemission and resonance photoemission at a lower resolution of around 200 meV. All spectra are referenced to a Fermi edge spectrum recorded from the cleaned metal sample plate and, where appropriate, normalized to the I_0 (flux) monitor of the beamline. The samples were mounted on a copper and tantalum sample plate on a He-cooled manipulator using Ag-loaded epoxy resin. The lowest attainable sample temperature was 13 K; resistive heating was used to explore temperatures up to 450 K. The surfaces of the crystals to be studied were cleaned for UHV measurements by fracturing the crystals parallel to their large (0 0 1) faces [1,20] using a diamond file in vacua of 10^{-10} mbar or lower. We regard the information obtained from these surfaces as effectively angle integrated. The surfaces of lanthanide cobaltites are generally unstable to surface degradation in UHV. We have studied the surface degradation reaction previously, and have found (through dosing experiments) that it is usually associated with the formation of surface hydroxide by adsorption of water or OH^- from the residual vacuum [11]. This is characterised by a progressive growth of peaks at around 9 eV and 5 eV binding energy (BE) (arising from the 1π and 3σ molecular orbitals of OH). Here, these signals were monitored as a function of time after fracturing, and the sample was recleaned (recovering the initial spectrum) when significant changes were noted (typically after several hours in UHV).

3. Results and discussion

3.1. General features of the valence band spectra

Fig. 1 shows valence band EDC spectra of Ln-112 (Ln = Gd) and Ln-114 (Ln = Yb) recorded at room temperature and a photon energy of 21 eV.

The spectra are normalized to the incident photon flux. Both oxides show a valence band around 9 eV wide, with two main features at around 4–5 eV and 9 eV BE. In the case of the double perovskite cobaltite Gd-112, shoulders appear near the valence band maximum (VBM) at around 0.75 eV and 2.5 eV BE. It has been shown previously that in the case of Gd-112, the peaks A_1, B_1 and C_1 contain contributions from O 2p and Co 3d states whereas D_1 shows mainly rare-earth 4f character [1]. We may anticipate similar origins for the valence band states in Yb-114 (discussed further in Section 3.2). Features labelled A (1 eV BE), B (5 eV BE) and C (9 eV BE) of Yb-114 lie at similar binding energy positions to A_1, C_1 and

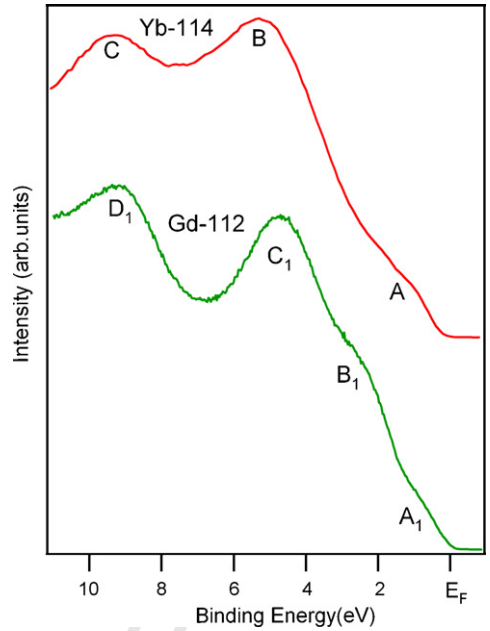

Fig. 1. Valence band spectra of Gd-112 ($\delta \approx 0.5$) and Yb-114 ($\delta \approx 0.2$) cobaltites. The spectra are recorded at room temperature and a photon energy of 21 eV.

D_1 of Gd-112 respectively. Feature B_1 of Gd-112 is missing in the valence band of Yb-114. The missing feature corresponds to one that has been previously tentatively assigned to the Co^{3+} LS state in an octahedral environment [1], on the basis of its similarity to the valence band photoemission spectrum of $LaCoO_3$ [11]. As no octahedral LS Co^{3+} states exist in Ln-114 for $\delta \approx 0.2$, the absence of this feature acts as useful confirming evidence of its assignment to octahedral LS Co^{3+}. The other difference lies in the density of states (DOS) close to the Fermi energy E_F. Gd-112 has a very small density of states close to E_F at room temperature, as it is close to the MI transition [1]. This increases as temperature is raised, as discussed in Section 3.3. In contrast, in Yb-114, there is no DOS at E_F; the valence band maximum lies at approximately 0.2 eV BE. This is consistent with semiconducting behaviour for Yb-114. No DOS at E_F was observed for Yb-114 in the temperature range 120–300 K.

3.2. Resonant photoemission of Yb-114

The direct photoemission process for a rare-earth configuration $4f^n$ can be written as:

$$4d^{10}4f^n + h\nu \rightarrow 4d^{10}4f^{n-1} + e^-. \quad (1)$$

Resonant photoemission is caused by a coherent superposition of this and the indirect channel opened up at resonance:

$$4d^{10}4f^n + h\nu \rightarrow \{4d^9 4f^{n+1}\}^* \rightarrow 4d^{10}4f^{n-1} + e^-, \quad (2)$$

where * denotes an excited state. This corresponds to creation of an intermediate 4d hole state which decays through a radiationless super Coster-Krönig (sCK) Auger recombination to give the same final state as the direct process. The cross section enhancement is very effective at the 4d → 4f giant resonance, providing a sensitive method of determining the 4f contribution to the valence band DOS.

Fig. 2 shows constant initial state (CIS) spectra for Yb-114, taken in the photon energy interval 170–215 eV, encompassing the Yb 4d → 4f resonance (around 182 eV). The BE positions selected for the CIS scans are shown in the inset valence band spectrum.

Strong resonant behaviour is observed for features C and D, with weaker resonances to higher binding energy, particularly in the region of features G and H. No resonance can be detected for the

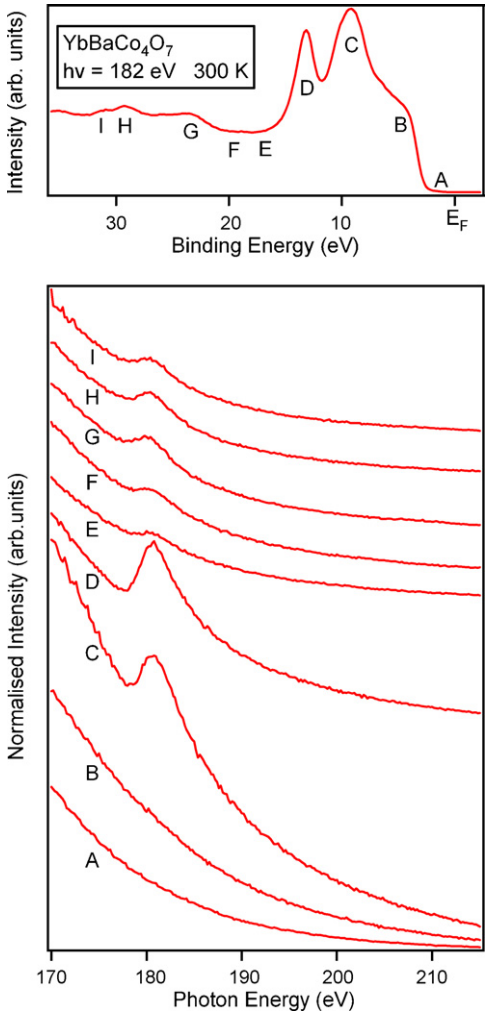

Fig. 2. CIS spectra of Yb-114 ($\delta \approx 0.2$) recorded over the photon energy range 170–215 eV (passing through the Yb 4d → 4f threshold), obtained for selected initial states A–I in the valence band. The spectra are normalized to the incident photon flux and were recorded at 300 K. The BE positions of features A–I are labelled in the inset.

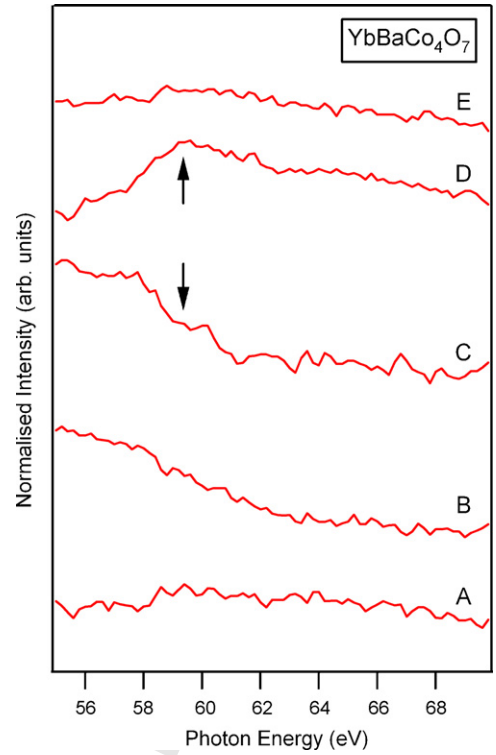

Fig. 3. CIS spectra from Yb-114 ($\delta \approx 0.2$) recorded over the photon energy range 55–70 eV (passing through the Co 3p → 3d threshold), obtained for selected initial states A–E in the valence band. Arrows indicate the positions of the resonance and anti-resonance observed for features D and C, respectively. The spectra are normalized to the incident photon flux and were recorded at 300 K. The BE positions of features A–E are labelled in the inset to Fig. 2.

lower binding energy valence band states (A and B). We conclude that the Yb 4f contribution to the valence band states is located mainly in the range 10–13 eV BE, with a contribution from the Yb 5p states in the range 25–30 eV BE. There is no Yb 4f contribution in the vicinity of the Fermi energy. This is consistent with an oxidation state of Yb^{3+} ($4f^{13}$) in Yb-114 [22]. Resonant photoemission of Yb^{2+} (f^{14}) shows a large DOS close to E_F in the BE range 0–3 eV [22], which is not observed here.

Similar experiments at the Ba 4d → 4f threshold (not shown) show the Ba states to be located in the 10–15 eV BE range, as in Ln-112 [1], while experiments at the O 2s → 2p threshold (not shown) show that features A–C (in particular B) have O character, again similar to the behaviour found in Ln-112 [7]. We note that the observation of any enhancement at this threshold implies the transfer of some electron density from O to the cation (here Co), creating so-called 'ligand-hole' states typical of highly correlated oxides [11], as otherwise the O 2p states are full, and resonant excitation cannot occur.

The contribution of Co states to the valence band DOS may be probed using the Co 3p → 3d resonance at around 62 eV, although the cross section is much lower than the 'giant' Ln 4d → 4f resonances. Fig. 3 shows CIS spectra from Yb-114 recorded over the photon energy range 55–70 eV, passing through the Co 3p → 3d threshold. The BE positions of the points A–E are shown in Fig. 2.

The spectra were recorded at room temperature and are normalized to the incident photon flux. Features A and E reveal no clear resonance effect. As the spectral intensity at feature A is very small and the Co 3p → 3d resonance is weak, we cannot conclude whether or not a resonance is absent in this case. A marked Co 3p → 3d resonance for feature D can be seen in the 57–62 eV photon energy range (marked by an arrow in Fig. 3). A dip in the CIS spectrum, related to feature C (and possibly also to B), at approximately 59 eV photon energy (also marked by an arrow in Fig. 3) reveals an anti-resonance. This destructive interference, which takes place when one of the photoemission channels is suppressed, has been observed in the valence band photoemission of a number of correlated oxides, including cuprates and nickelates [23,24]. Typically, resonance of so-called 'satellite' features at around 12 eV BE has been associated with an unscreened photoemission final state $3d^{n-1}$, whereas the majority valence band structure arises from the screened final state $3d^n\underline{L}^1$ (where $\underline{L}$ implies a ligand hole, *i.e.* in this case, electron transfer from an O anion) [23,24]. This is consistent with the behaviour observed here, with a resonance at around 13 eV BE, and anti-resonance in the main part of the valence band (5–10 eV BE). Thus the main part of the valence band observed in photoemission arises from screened final states, where electrons have transferred from the ligand O ion to the central Co ion, consistent with the observation of resonant enhancement at the O 2s → 2p threshold. Overall, we may conclude that the Co 3d states contribute to the valence band spectrum in the range 5–13 eV BE, and we cannot rule out a contribution to the states closest to E_F (point A).

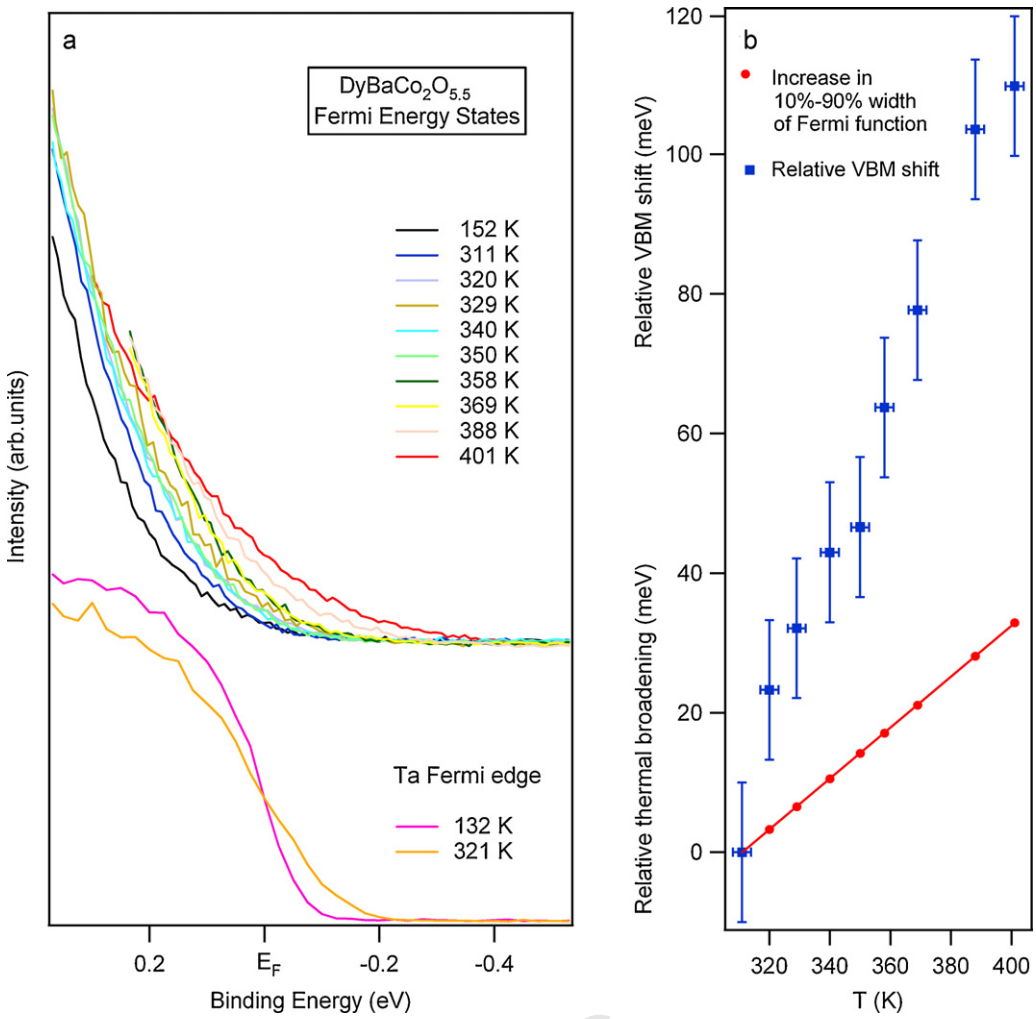

Fig. 4. (a) High-resolution photoemission spectra of the low BE states of Dy-112 ($\delta \approx 0.5$) as a function of temperature. The photon energy is 33 eV and the experimental resolution (analyser + monochromator) is fixed at 115 meV. The spectra of Dy-112 are normalized to the incident photon flux (and their intensity is expanded by a factor of approximately 50 compared with Fig. 1). For comparison, Fermi cut-off spectra of clean Ta in contact with the sample are also shown. (b) The shift of the VBM of Dy-112 ($\delta \approx 0.5$) with temperature, relative to the measured VBM position at 311 K (squares). The expected increase in the 10–90% width of a metal Fermi cut-off due to thermal broadening relative to that at 311 K (at fixed experimental resolution of 115 meV) is also shown (dots).

3.3. *Variation in the DOS at E_F with temperature*

As noted above, we observed no DOS at E_F for Yb-114 in the temperature range 120–300 K. In contrast, for Ln-112, we typically observe a gradual but very small enhancement in the DOS at E_F with increase in temperature, particularly in the range 300–400 K, where the MI transitions of most of the later series Ln-112 oxides are expected [2,6,7]. A typical example is shown in Fig. 4(a), for a crystal of Dy-112 which has been oxygen annealed after synthesis to achieve an oxygen content close to $\delta = 0.5$; here we expect the MI transition at around 326 K [25]. Typical spectra of a metal Fermi cut-off, recorded during the same experiment are also shown for comparison in Fig. 4(a).

The overall resolution of these spectra (including the effect of thermal broadening) rises from 128 meV (at 152 K) to 164 meV (at 311 K) and 190 meV (at 401 K). The shift of the VBM towards E_F with increasing temperature between 152 K and 311 K is around 34 meV, and is therefore attributable to thermal broadening. However, in the region of the MI transition (311–401 K), the observed shift is significantly larger and cannot be explained solely by the increase in thermal broadening. This demonstrated in Fig. 4(b) where we plot the relative shift of the VBM against temperature, and compare it with the increase in thermal broadening over the same temperature range. Our results are consistent with those of Takubo et al. [26] for Tb-112, and our own previous measurement for Gd-112 [7]. Changes observed in the intensity of feature B with temperature (not shown) are also very gradual and slight. These observations suggest that the MI transition does not occur via a sudden switch from LS to HS as proposed by Frontera et al. [6], but is consistent with a more gradual switch in the temperature-determined equilibrium between LS, IS and HS states [10,11].

4. Conclusions

Resonant photoemission reveals strong general similarities in the atomic character of the valence band states of Ln-112 and Ln-114. In both cases, the valence band is made up primarily of Co 3d and O 2p states, with the Ln 4f character lying to higher binding energy (below around 9 eV BE). However, differences are observed in the DOS around the VBM. In particular, a feature at around 2.5 eV binding energy, previously tentatively associated with LS Co^{3+} in octahedral sites, is missing in the case of Ln-114 (which has no Co in octahedral sites for low δ). We find the VBM at around 0.2 eV BE, with no DOS at E_F in the case of Ln-114, suggesting semiconducting behaviour. In Ln-112 containing late series Ln elements, a slight and gradual increase in DOS at E_F with temperature is observed,

particularly in the region of the MI transition (typically 300–400 K) [7,26], suggesting that the MI transition does not occur via a sudden LS–HS spin flip.

Acknowledgements

We thank the Royal Society of Great Britain for the award of a collaborative research grant between ISSSP Minsk and the University of Manchester. The sample preparation in Minsk was partly supported by the Belarussian State Fund for Basic Research under grant No F09K-017. H.M.R. thanks the University of Manchester for a postgraduate scholarship.

References

[1] W.R. Flavell, A.G. Thomas, D. Tsoutsou, A.K. Mallick, M. North, E.A. Seddon, C. Cacho, A.E.R. Malins, S. Patel, R.L. Stockbauer, R.L. Kurtz, P.T. Sprunger, S.N. Barilo, S.V. Shiryaev, G.L. Bychkov, Phys. Rev. B 70 (2004) 224427.
[2] A. Maignan, C. Martin, D. Pelloquin, N. Nguyen, B. Raveau, J. Solid State Chem. 142 (1999) 247–260.
[3] Z.X. Zhou, S. McCall, C.S. Alexander, J.E. Crow, P. Schlottmann, S.N. Barilo, S.V. Shiryaev, G.L. Bychkov, R.P. Guertin, Phys. Rev. B 70 (2004) 024425.
[4] A.A. Taskin, A.N. Lavrov, Y. Ando, Phys. Rev. B 71 (2005) 134414.
[5] S. Streule, A. Podlesnyak, J. Mesot, M. Medarde, K. Conder, E. Pomjakushina, E. Mitberg, V.J. Kozhevnikov, J. Phys. Condens. Matter 17 (2005) 3317–3324.
[6] C. Frontera, J.L. Garcia-Munoz, A. Llobet, M.A.G. Aranda, Phys. Rev. B 65 (2002) 180405.
[7] S.N. Barilo, S.V. Shiryaev, G.L. Bychkov, A.S. Shestak, W.R. Flavell, A.G. Thomas, H.M. Rafique, Y.P. Chernenkov, V.P. Plakhty, E. Pomjakushina, K. Conder, P. Allenspach, J. Cryst. Growth 310 (2008) 1867–1874.
[8] M.A. Korotin, S.Yu. Ezhov, I.V. Solovyev, V.I. Anisimov, D.I. Khomskii, G.A. Sawatzky, Phys. Rev. B 54 (1996) 5309–5316.
[9] M. Imada, A. Fujimori, Y. Tokura, Rev. Mod. Phys. 70 (1998) 1039–1263.
[10] K. Asai, A. Yoneda, O. Yokokura, J.M. Tranquada, G. Shirane, K. Kohn, J. Phys. Soc. Jpn. 67 (1998) 290–296.
[11] A.G. Thomas, W.R. Flavell, P.M. Dunwoody, C.E.J. Mitchell, S. Warren, S.C. Grice, P.G.D. Marr, D.E. Jewitt, N. Khan, S.W. Downes, D. Teehan, E.A. Seddon, K. Asai, Y. Koboyashi, N. Yamada, J. Phys. Condens. Matter 12 (2000) 9259–9279.
[12] M. Valldor, M. Anderson, Solid State Sci. 4 (2002) 923–931.
[13] E.V. Tsipis, D.D. Khalyavin, S.V. Shiryaev, K.S. Redkina, P. Núñez, Mater. Chem. Phys. 92 (2005) 33–38.
[14] M. Valldor, N. Hollman, J. Hemberger, J.A. Mydosh, Phys. Rev. B 78 (2008) 024408.
[15] W. Schweika, M. Valldor, P. Lemmens, Phys. Rev. Lett. 98 (2007) 067201.
[16] A. Huq, J.F. Mitchell, H. Zheng, L.C. Chapon, P.G. Radaelli, K.S. Knight, P.W. Stephens, J. Solid State Chem. 179 (2006) 1136–1145.
[17] O. Chmaissem, H. Zheng, A. Huq, P.W. Stephens, J.F. Mitchell, J. Solid State Chem. 181 (2008) 664–672.
[18] G.L. Bychkov, S.V. Shiryaev, A.G. Soldatov, A.S. Shestak, S.N. Barilo, D.V. Sheptyakov, K. Conder, E. Pomjakushina, A. Podlesnyak, A. Furrer, R. Bruetsch, Cryst. Res. Technol. 40 (2005) 395–399.
[19] G.L. Bychkov, S.N. Barilo, S.V. Shiryaev, D.V. Sheptyakov, S.N. Ustinovich, A. Podlesnyak, M. Baran, R. Szymczak, A. Furrer, J. Cryst. Growth 275 (2005) e813–e818.
[20] A.N. Bludov, S.L. Gnatchenko, R. Szymczak, H. Szymczak, S.N. Barilo, G.L. Bychkov, S.V. Shiryaev, Low Temp. Phys. 35 (2009) 971–973.
[21] M. Bowler, J.B. West, F.M. Quinn, D.M.P. Holland, B. Fell, P.A. Hatherly, I. Humphrey, W.R. Flavell, B. Hamilton, Surf. Rev. Lett. 9 (2002) 577–581.
[22] *e.g.* T. Okane, S. Fujimori, K. Mamiya, J. Okamoto, Y. Muramatsu, A. Fujimori, Y. Nagamoto, T. Koyanagi, J. Phys. Condens. Matter 15 (2003) S2197–S2200.
[23] W.R. Flavell, J. Hollingworth, J.F. Howlett, A.G. Thomas, Md.M. Sarker, S. Squire, Z. Hashim, M. Mian, P.L. Wincott, D. Teehan, S. Downes, F.E. Hancock, J. Synchrotron Radiat. 2 (1995) 264–271.
[24] J. Ghijsen, L.H. Tjeng, H. Eskes, R.L. Johnson, G.A. Sawatzky, Phys. Rev. B 42 (1990) 2268–2274.
[25] M. Lafkioti, E. Goering, S. Gold, G. Schütz, S.N. Barilo, S.V. Shiryaev, G.L. Bychkov, P. Lemmens, V. Hinkov, J. Deisenhofer, A. Loidl, New J. Phys. 10 (2008) 123030.
[26] K. Takubo, J.Y. Son, T. Mizokawa, M. Soda, M. Sato, Phys. Rev. B 73 (2006) 075102.